A six-dimensional potential energy surface for Ru(0001)(2×2):CO

Gernot Füchsel, Jean Christophe Tremblay, and Peter Saalfrank

Citation: The Journal of Chemical Physics **141**, 094704 (2014); doi: 10.1063/1.4894083
View online: http://dx.doi.org/10.1063/1.4894083
View Table of Contents: http://scitation.aip.org/content/aip/journal/jcp/141/9?ver=pdfcov
Published by the AIP Publishing

A six-dimensional potential energy surface for Ru(0001)(2×2):CO

Gernot Füchsel,[1] Jean Christophe Tremblay,[2] and Peter Saalfrank[1,a)]
[1]*Institut für Chemie, Universität Potsdam, Karl-Liebknecht-Straße 24-25, D-14476 Potsdam-Golm, Germany*
[2]*Institut für Chemie und Biochemie - Physikalische und Theoretische Chemie, Freie Universität Berlin, Takustr. 3, 14195 Berlin, Germany*

(Received 15 June 2014; accepted 12 August 2014; published online 3 September 2014)

We present a new global ground state potential energy surface (PES) for carbon monoxide at a coverage of 1/4, on a rigid Ru(0001) surface [Ru(0001)(2×2):CO]. All six adsorbate degrees of freedom are considered. For constructing the PES, we make use of more than 90 000 points calculated with periodic density functional theory using the RPBE exchange-correlation functional and an empirical van der Waals correction. These points are used for interpolation, utilizing a symmetry-adapted corrugation reducing procedure (CRP). Three different interpolation schemes with increasing accuracy have been realized, giving rise to three flavours of the CRP PES. The CRP PES yields in agreement with the DFT reference and experiments, the *atop* position of CO to be the most stable adsorption geometry, for the most accurate interpolation with an adsorption energy of 1.69 eV. The CRP PES shows that diffusion parallel to the surface is hindered by a barrier of 430 meV, and that dissociation is facilitated but still activated. As a first "real" application and further test of the new potential, the six-dimensional vibrational Schrödinger equation is solved variationally to arrive at fully coupled, anharmonic frequencies and vibrational wavefunctions for the vibrating, adsorbed CO molecule. Good agreement with experiment is found also here. Being analytical, the new PES opens an efficient way towards multidimensional dynamics. © *2014 AIP Publishing LLC*. [http://dx.doi.org/10.1063/1.4894083]

I. INTRODUCTION

A detailed knowledge of interatomic interactions is essential to achieve a microscopic understanding of chemical processes and dynamics in molecular systems. Not only stationary points such as minima or transition states are required, but also large portions of a multidimensional potential energy surface (PES) can be visited during chemical reactions and should therefore be known. Experimental knowledge on stable geometries, energetics, thermodynamics and even kinetics is often good. This is not the case for non-stationary points and real-time dynamics, where, however, time-resolved techniques such as pump-probe spectroscopy[1] have improved our understanding of chemical change.

Here, theory can be of invaluable additional help. On its most fundamental level, molecular quantum mechanics, theory often takes all the steps from electronic structure over vibrational and thermodynamical data analysis, to dynamical simulations of chemical reactions.[2–8] For this latter purpose, an *a priori* construction of multidimensional potential energy surfaces is a valuable tool. A popular alternative to using global potentials, valid for classical dynamics at least, is the "on-the-fly" characterization of electronic structure, energies, and forces. The pointwise determination of these quantities, however, can be costly in particular when meaningful statistical averages over trajectories are required. There are several further advantages of a global PES: It allows one to determine reaction barriers along several pathways prior to any dynamical simulation; thermodynamic and also quantum mechanical features are easily accessible; at least classical dynamics becomes extremely efficient computationally. In summary, a global PES is very useful—provided it can be constructed. This task becomes more complex with increasing system size, in particular when (first principles) electronic structure methods rather than force fields are to be used.

Two widespread approaches towards constructing a PES are by using analytical functions based on sound physical modeling,[9–12] or by calculating a large number of *ab initio* points interpolated using various unbiased mathematical procedures without immediate physical reasoning.[13–15] Another approach is taken in neural networks, for example, see Refs. 16–21.

In this work, we present a global six-dimensional potential energy surface for a CO molecule interacting with a rigid Ru(0001) surface. The Ru(0001):CO system was subject to many experimental investigations on dissociative adsorption,[22] thermal and laser-induced desorption,[22–29] electron-stimulated desorption and dissociation,[30] as well as adsorption/desorption on/from oxygen-precovered Ru(0001).[31,32] In previous theoretical work, the nature and strength of adsorptive bonding of CO on the surface was of interest,[33] or the mapping of phase diagrams.[28] Only in rare cases, reaction dynamics were treated, then with reduced-dimensional potential energy surfaces only.[26]

Part of the interest on Ru:CO is practical due to aspects related to heterogeneous catalysis, however, also more fundamental questions arise. In recent experiments, for example, using X-ray lasers as probes, the weakening of the CO-surface bond and associated electronic structure changes after femtosecond-laser excitation of Ru(0001):CO could be

a)Email: peter.saalfrank@uni-potsdam.de

followed in real time.[34] It was shown that transient, physisorptive precursor states, possibly created by hot-electron mediated dissipative dynamics, participate in the process. These hallmark experiments require tremendous effort to provide evidence of short-lived transient species in surface-activated processes. An adequate level of theoretical treatment is mandatory to keep pace with the experimental progress made in the field. It is the aim of this work to overcome some of the current theoretical limitations by computing an accurate PES for CO on Ru(0001). This should finally allow for treating complex, e.g., hot-electron mediated and dissipative dynamics for Ru(0001):CO of the type as demonstrated in Ref. 34, similar to previous theoretical work on Ru(0001):H.[35]

In order to construct a PES, we employ periodic density functional theory for CO in different orientations on the Ru surface. The DFT points are interpolated using the so-called corrugation reducing procedure (CRP).[15] The method being variational, a desired high accuracy can be achieved, while keeping the number of interpolation points modest by using "reference potentials." The CRP was previously applied with great success for various global PESs of atoms and diatomic homonuclear molecules at metal surfaces.[13–15,35–38]

Here we first of all demonstrate that the CRP is also appropriate to obtain 6D PESs for diatomic heteronuclear molecules. When constructing potential energy surfaces by using interpolation procedures, an important question is how many points need to be included. Two decisive criteria are the performance for data points outside the interpolation set, and the performance of the PES in reproducing properties. In what follows both criteria will be tested, the latter by comparing vibrational frequencies and wavefunctions of the adsorbed molecules. This is done for three different versions of the PES, as obtained with different numbers of DFT points used in the CRP interpolation scheme.

The paper is organized as follows. In Sec. II, we describe the model and the DFT methodology used. In Sec. III, the corrugation reducing procedure is explained in detail as well as interpolation techniques for the construction of the three different PESs under study. The accuracy of the PESs is tested by using DFT points outside the interpolation set in Sec. IV, and by performing a six-dimensional vibrational mode analysis in Sec. V. In Sec. VI, we take a closer look into features of the PES not considered up till then. Finally, Sec. VII summarizes this work.

II. MODEL AND METHOD

In the following, we employ a three-layer slab model with one CO molecule per (2×2) supercell, corresponding to a coverage of 1/4 (cf. Fig. 1).

A vacuum gap 25.8 Å wide was chosen. Periodic DFT calculations were carried out to obtain data points, using the Vienna *ab initio* Simulation Package VASP.[39,40] The gradient-corrected RPBE functional[41] was used, and ion cores were described with standard pseudopotentials.[39,42] We employed a 9 × 9 × 1 Γ-centered Monkhorst-Pack grid and plane augmented wave functions with a kinetic energy cutoff of 400 eV.

When optimizing the bulk Ru crystal with these computational parameters we obtain a shortest Ru-Ru distance of $d = 2.725$ Å and a c/d-ratio of 1.58, where c is the distance between the first to the third layer. Hence in the bulk, Ru layers are separated by 2.153 Å. The corresponding experimental values are $d = 2.700$ Å and 1.584 for c/d, respectively,[43] giving a layer separation of about 2.14 Å. In the three-layer slab model, when optimizing the top layer and keeping the two lower layers fixed, the upper layer moves inward by 0.096 Å, giving a separation between the two topmost layers of 2.057 Å.

This relaxed slab was then used, without further lattice reoptimizations, as a starting point for constructing the 6D PES for Ru(0001):CO. The (2×2) three-layer slab with one CO contains 14 atoms. The six degrees of freedom are the usual center of mass position with its two lateral components X and Y relative to a Ru reference atom, and the surface-molecule distance Z, further the interatomic distance r, the polar angle $\theta \in [0, \pi]$, and, finally, the azimuthal angle $\phi \in [0, 2\pi]$, cf. Fig. 1 and Sec. III below.

Before elaborating on details of the PES and its evaluation, we note that at its global minimum, CO adsorbs *on-top* of a Ru atom, with the C-end pointing down. The molecule-surface distance is $Z_{eq} = 2.592$ Å, and $r_{eq} = 1.168$ Å. The other four coordinates are $X = Y = \phi = \theta = 0$. An adsorption energy $E_{ads} = 1.43$ eV is found, when no van der Waals (vdW) interactions were accounted for.

As shown in Ref. 44 for the system Ru(0001):H_2, the inclusion of vdW interaction can have an impact on PES properties. Since this might affect also results for CO on Ru(0001), we adopted the semiempirical D2 correction scheme of

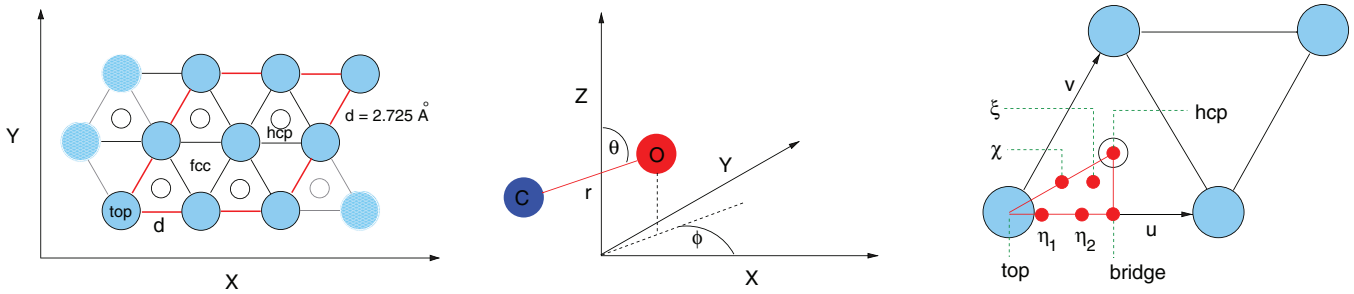

FIG. 1. Coordinate system for CO on a Ru(0001) surface. Left: Hexagonal Ru lattice, indicated are *top*, *fcc*, and *hcp* sites, the shortest Ru-Ru distance d and the (2×2) cell. Middle: Definition of the center of mass position X, Y, Z, the interatomic distance r, the polar angle $\theta \in [0, \pi]$, and the azimuthal angle $\phi \in [0, 2\pi]$ for CO. Right: Seven adsorption sites (red dots) in the (u, v)-plane which were used for various interpolation procedures (see text). Also shown are the $\vec{u}$ and $\vec{v}$ vectors with the length $|\vec{u}| = |\vec{v}| = d$. The transformation from (X, Y) to (u, v) coordinates is $u = X - \frac{Y}{\sqrt{3}}$ and $v = \frac{2}{\sqrt{3}} Y$, respectively.

Grimme.[45] D2 and similar schemes tend to overestimate the interaction of the adsorbate with lower-lying layers in case of metal surfaces.[46] Therefore, in accordance with previous experience,[46] the vdW interaction between CO and the top Ru layer only was considered. With these vdW corrections, the classical equilibrium coordinates shift only marginally (in the order of less than 0.001 Å), while the adsorption energy increases to 1.69 eV. All of these values agree well with data obtained from a direct optimization (at a fixed Ru lattice), with VASP. With vdW interactions included, for example, the optimal geometry corresponds to Z_{eq}(VASP) = 2.586 Å and r_{eq}(VASP)=1.171 Å, respectively. The adsorption energies agree also well with the CRP potential values, and so do effects due to vdW forces.

The geometries obtained from the CRP PES are also in full agreement with previous experiments,[47] where Z_{eq} = 2.628 ± 0.05 Å and r_{eq} = 1.10 ± 0.05 Å were found. Also the computed adsorption energies E_{ads} are compatible with experiments. In Ref. 29, E_{ads} was given as 1.65 eV for coverages comparable to those studied here.

In passing, we note that for the bond energy of the free CO molecule (calculated at $Z = 5.1$ Å and parallel to the surface), we obtain 11.24 eV which is again in good agreement with the experimental value of 11.11 eV.[48] For the free CO molecule, a C-O distance of $r_{eq} = 1.148$ Å is found.

Further details of the PES, away from its global minimum will be outlined in Sec. VI. A first conclusion from our observations so far is that the RPBE functional (and the 6D PES derived from it) performs well for the adsorption of CO on Ru(0001).

III. CONSTRUCTION OF THE POTENTIAL ENERGY SURFACE

To represent the global potential energy surface (PES) for Ru(0001)(2×2):CO, we make use of the so-called corrugation reducing procedure.[15] Here, the PES $V(X, Y, Z, r, \theta, \phi)$ is decomposed into an interaction potential $I(X, Y, Z, r, \theta, \phi)$ and reference potentials $V_{ref}(x, y, z)$ that depend on atomic coordinates,

$$V(X, Y, Z, r, \theta, \phi) = I(X, Y, Z, r, \theta, \phi) + V_{ref}(x_C, y_C, z_C) + V_{ref}(x_O, y_O, z_O). \quad (1)$$

The reference potentials can be arbitrarily chosen but should roughly represent the general form of the CO potential, especially in its repulsive regions. For our purpose, we use a sum of C-Ru and O-Ru potentials, respectively, in a reference cluster model,

$$V_{ref}(x, y, z) = \sum_{i=1}^{N_{clust}} V_{top}(r_i), \quad (2)$$

where $r_i = \sqrt{(x - x_i)^2 + (y - y_i)^2 + (z - z_i)^2}$ is the distance between the C or O atom and the ith Ru atom. The cluster contains 127 ruthenium atoms in one layer, arranged in six concentric Ru hexagons around a central Ru atom. The one-dimensional reference potentials V_{top} are calculated at *top*-position (see Figure 1) along the z-direction by using periodic DFT and the RPBE functional. For both, carbon and oxygen, we employ spin-polarized calculations on a (2×2) cell. The atomic reference potentials are made periodically along x and y by using a mapping procedure. Before evaluating V_{ref}, each $\{x, y\}$-position is mapped back to its corresponding $\{x', y'\}$-position close to the center atom of the cluster. For the new position applies $-d < x' - y'/\sqrt{3} < d$ and $-\sqrt{3}d/2 < y' < \sqrt{3}d/2$, where d is the shortest Ru-Ru distance. In our work, it turns out to be useful to choose such simple reference potentials. More sophisticated solutions as suggested in Refs. 13 and 15 yield a spurious behaviour of the potential near the global minimum geometry.

TABLE I. Number N_{cut} of calculated two-dimensional cuts (r, Z) at different adsorption sites. The sum of all N_{cut} values is 224. Each cut contains 408 DFT points with $r \in [0.725, 2.725]$ Å and $Z \in [1.65, 5.1]$ Å, for steps $\Delta r = 0.125$ Å and $\Delta Z = 0.15$ Å, respectively.

	top	η_1	η_2	*brg*	*hcp*	χ	ζ
N_{cut}	12	37	37	22	17	37	62

To provide an accurate representation of the six-dimensional PES, we calculate 224 two-dimensional (2D) cuts along $r \in [0.725, 2.725]$ Å and $Z \in [1.65, 5.1]$ Å on an equidistant grid for different geometries tilted along θ and ϕ at seven selected adsorption sites (X, Y combinations) as shown in Fig. 1. Each cut contains 408 DFT points, corresponding to 224 × 408 = 91392 points in total. The 2D grid spacings were $\Delta r = 0.125$ Å and $\Delta Z = 0.15$ Å, respectively. The number of 2D cuts (N_{cut}) calculated for different adsorption sites are listed in Table I. This number depends on the symmetry of the site for a displacement of the CO molecule along ϕ. Concerning the symmetry issue we note that our periodic DFT calculations have shown that energies are very similar at *hexagonal closed package* (*hcp*) and *face centered cubic* (*fcc*) sites. To reduce the computational effort, we therefore do not distinguish between them and assume C_{6v}-symmetry for the CO molecule at *top*, C_{3v}-symmetry at *hcp*, C_{2v}-symmetry at *bridge* (*brg*), C_1-symmetry at ζ, and C_s-symmetry at η_1, η_2 and ξ positions, respectively. To sample the adsorbate motion along the angular degrees of freedom θ and ϕ, we choose grid spacings $\Delta\theta = \Delta\phi = \pi/6$. For points where no symmetry can be used such as ζ, this corresponds to $N_{cut} = (\pi/(\pi/6) - 1) \times 2\pi/(\pi/6) + 2 = 62$ points per (r, Z, X, Y) value.

After substraction of the reference potentials from the DFT points, we obtain the six-dimensional interaction potential $I(X, Y, Z, r, \theta, \phi)$ by using the following interpolation sequences:

1. Interpolation along r and Z by using a 2D spline interpolation as presented in Ref. 49.
2. Interpolation along θ by using a one-dimensional Fourier interpolation.
3. Interpolation along X, Y, ϕ by using a coupled three-dimensional symmetry-adapted Fourier interpolation.

In order to obtain proper derivatives of the potential with respect to θ at low-symmetry sites and $\theta = 0$ and 180°, we inter-

polate θ in the interval $[0, 2\pi]$ and make use of the following property:

$$V(X, Y, Z, r, \theta \in [\pi, 2\pi], \phi) = V(X, Y, Z, r, \theta \in [0, \pi], \phi + \pi). \quad (3)$$

Note, this applies to the interpolation only. The physical definition $\theta \in [0, \pi]$ remains unchanged. We extend the CRP PES to large Z values ($Z > 5.1$ Å) by mixing the CRP interaction potential and the CRP asymptotic potential $I_{gas}(r)$ so that the resulting PES equals the potential $V_{\text{gas}}(r)$ in gas phase. The resulting modified 6D interaction potential is

$$I^{mod}(X, Y, Z, r, \theta, \phi) = \begin{cases} I(X, Y, Z, r, \theta, \phi)(1 - f(Z)) + I_{gas}(r) f(Z) & Z_{min} \le Z \le Z_{max} \\ I_{gas}(r) & Z > Z_{max}, \end{cases} \quad (4)$$

where $f(Z) = \frac{1}{2} + \frac{1}{2}\cos(\frac{Z_{max} - Z}{Z_{max} - Z_{min}}\pi)$ and $I_{\text{gas}} = V_{\text{gas}}(r) - V_{ref}(x_C, y_C, z_C) - V_{ref}(x_O, y_O, z_O)$. We choose $Z_{max} = 5.1$ Å and $Z_{min} = 4.6$ Å.

Employing group theory as done for example in Ref. 50, we derived three different expressions for the three-dimensional symmetry-adapted Fourier interpolation, corresponding to increasing numbers of interpolation points in the (u, v)-plane (cf. Fig. 1). As a result, we obtain three different variants of the potential, with increasing accuracy, called V_{low}, V_{med}, and V_{high} in the following. For all of these, we distinguish between surfaces with and without van der Waals corrections included. For V_{low}, we used three interpolation points located at *top*, *brigde*, and *hcp* sites. The potential V_{med} is of medium quality and built with an additional point located at χ position, that is, between *top* and *hcp* sites. Finally, V_{high} is a high-quality surface and constructed by using all seven adsorption sites as shown in Fig. 1. With increasing quality the different potentials become also computationally more demanding which can play a role, e.g., in molecular dynamics. The calculation of V_{low} for a given point is about 4.5 and that of V_{med} about 2.5 faster than that of V_{high}.

IV. ACCURACY OF THE POTENTIAL ENERGY SURFACE

In the following, we show that the CRP is an accurate and efficient representation of the global 6D PES for CO on Ru(0001). In order to test the accuracy of the PES, we first select 1200 random geometries of CO at Ru which were not used for the fitting procedure. For each of the points we calculate DFT energies (V_i^{DFT}), and compare them to the CRP potential values $V_i(X, Y, Z, r, \theta, \phi)$. As a measure for the performance of the CRP PES, we give the root mean square (RMS) deviation as a function of a maximal potential energy V_{max} (relative to the global potential minimum), below which test points were included:

$$\text{RMS} = \sqrt{\frac{1}{N-1}\sum_{i=1}^{N}\left[V_i(X, Y, Z, r, \theta, \phi) - V_i^{DFT}\right]^2}, \quad (5)$$

for all $V_i(X, Y, Z, r, \theta, \phi) \le V_{max}$.

Note, the random test set does not include geometries associated with energies below 500 meV.

The result is shown in Fig. 2, for the DFT points calculated with the pure RPBE functional, i.e., without vdW corrections, and the CRP PES being of "high" quality, also without vdW. (Test calculations showed that the inclusion of van der Waals forces gave very similar results.) As can be seen, the interpolation error for a cutoff $V_{max} = 2$ eV is around 23 meV (1st section of the figure). Up to this energy, most of "conventional" nuclear dynamics takes place, i.e., thermal or photoinduced desorption. Evaluating the RMS for all potential values lower than 6 eV, we still obtain a good accuracy with RMS = 60 meV (2nd and 3rd sections of the figure). With increasing potential values V_{max}, the interpolation error increases. But even for values up to 400 eV, the RMS is around 300 meV which is still very good. The interpolation error at a given V_{max} is lower than 2%. Overall, "chemical accuracy" (1 kcal/mol or 44 meV) for the interpolation error, is realized up to cutoff energies of about 3 eV.

In Fig. 3, as a second test, we show the performance of the CRP when used to describe multidimensional potential energy surfaces. In Fig. 3(a), we compare our CRP potential (red line) as a function of the rotational motion along angle θ for a point at the *bridge* site, to DFT calculations (black dots). The overall agreement is very good on the scale of typical energy variations. Closer inspection shows that our PES tends to underestimate the DFT reference slightly. A RMS value of 11.4 meV and a maximum error of around +20 meV (blue curve and symbols) was obtained.

In Fig. 3(b), a one-dimensional potential cut for the lateral motion from *bridge*-to-*bridge* along the *X*-direction is pictured when the CO molecule is oriented parallel to the surface. Also here the errors are very small, with a RMS value of only 1.3 meV.

Comparing potential energy differences between V_{low} and V_{med} relative to V_{high}, it turns out that the number of interpolation points in the (u, v)-plane has only a small effect on the accuracy of the potential certainly at low energy values. For all potential energies V_{max} lower than 2 eV, we find an RMS value of 1.8 meV in case of V_{med} and 2.0 meV in case of V_{low}, both relative to V_{high}. With increasing potential the corresponding RMS values increase up to about 150 meV and 300 meV, respectively. For the calculation

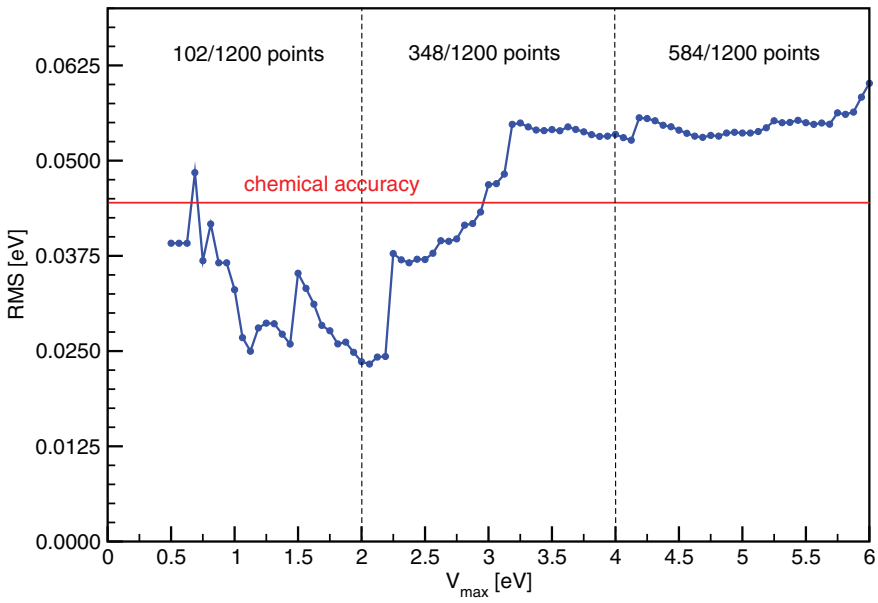

FIG. 2. Accuracy of the potential energy surface obtained with the pure RPBE functional (no vdW corrections, V_{high} in case of CRP). Shown is the RMS value (blue) as a function of a maximum potential value V_{max}, up to which test points have been considered. The red line represents an interpolation error of "chemical accuracy" (1 kcal/mol ∼ 44 meV). For the different segments, we give the number of DFT points we compare with.

of the RMS, 100 000 geometries were considered in this case.

V. VIBRATIONAL ANALYSIS

To benchmark the quality of the potential fit, we proceed to analyze the vibrations of the CO moiety. As a first test, the normal modes obtained using VASP are compared with the normal mode analysis of the fitted PES. For the former, the most stable adsorption site for Ru(0001)(2×2):CO in the *atop* position has been chosen.

The normal mode analysis gives the usual low-frequency T- (frustrated translation), medium-frequency R- (frustrated rotation), and S-modes (surface-CO mode), as well as the high-frequency CO-stretch mode, as can be seen from Table II. In case of the VASP normal mode analysis ("VASP" in the table), a step size of $\Delta = 0.015$ Å has been used for evaluating derivatives. It must be said that the results are quite

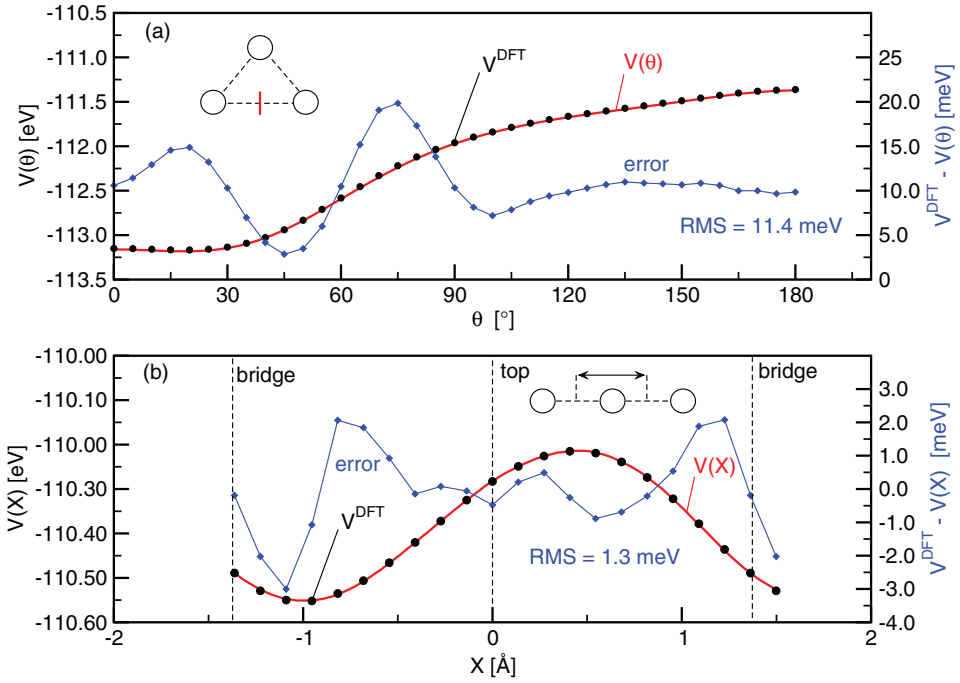

FIG. 3. Interpolated potential (red line) in comparison to DFT reference points (black circles). Shown is (a) a one-dimensional PES for the CO molecule rotating along $\theta \in [0, 180°]$ at the *bridge* site ($\{Z = 2.6$ Å, $r = 1.2$ Å, $\phi = 0°\}$, see inset) and (b) for a *bridge*-to-*bridge* motion along X when the molecule is oriented parallel to the surface ($\{Y = 0, r = 1.475$ Å, $Z = 2.25$ Å, $\theta = 90°, \phi = 0°\}$, see other inset). Also given are errors as a function of the displayed coordinates (blue squares) and RMS values.

TABLE II. Vibrational analysis for Ru(0001)(2 × 2):CO at its global minimum. Tabulated are wave numbers $\tilde{\nu}$ [cm^{-1}] obtained from a classical normal mode analysis (NMA) and quantum mechanical (QM) calculations for different vibrational modes, both for different-quality CRP PESs, with and without vdW interactions included. Comparison to a normal mode analysis with VASP is also given. In all cases, the Ru surface was kept rigid. Experimental values are shown for the different modes. The abbreviation "dnc" stands for "did not converge".

	Without vdW				With vdW			
	T-mode $\{\nu_X, \nu_Y\}$	R-mode $\{\nu_\theta, \nu_\phi\}$	S-mode ν_Z	CO-stretch ν_r	T-mode $\{\nu_X, \nu_Y\}$	R-mode $\{\nu_\theta, \nu_\phi\}$	S-mode ν_Z	CO-stretch ν_r
VASP	{27, 36}	{384, 384}	398	1957	{27, 36}	{387, 387}	416	1962
NMA, V_{low}	{100, 100}	{384, 389}	408	2095	{108, 108}	{389, 394}	414	2097
NMA, V_{med}	{54, 54}	{396, 400}	408	2095	{70, 71}	{403, 407}	414	2097
NMA, V_{high}	{54, 59}	{394, 398}	408	2095	{67, 71}	{400, 404}	414	2097
QM, V_{low}	96.4	378.7	396.0	2008.0	103.6	382.8	409.7	2012.4
QM, V_{med}	53.8	391.7	395.7	2008.0	66.3	397.1	409.6	2012.4
QM, V_{high}	47.9	388.5	397.9	2008.0	60.8	dnc	411.0	2012.4
Expt.	...	...	...	...	45[51] / 40 ± 8[52]	412[53,54]	445[55]	2010[56]

sensitive to the stepsize used in the computation, in particular for the T-mode, which should therefore be taken with care.

For the normal mode analysis of the CRP PES, labeled "NMA," the Hessian in mass-weighted coordinates is constructed. The (non-mass-weighted) second derivatives of the potential are obtained with different step sizes Δ ranging from 10^{-2} to 10^{-5} a_0. The results presented in Table II are converged, and the behaviour with respect to the step size is much more robust due to the analytical form of the potential fit. Further, all three different CRP PES V_{low}, V_{med}, and V_{high} have been tested, and the role of van der Waals interactions has been studied. A striking feature of the normal modes obtained from the PES is that the R-mode, the S-mode, and the CO-stretch frequencies are quite insensitive to both the quality of the underlying (u, v)-interpolation scheme and the inclusion of van der Waals corrections. Nonetheless, a small degeneracy lift remains in the R-mode due to numerical inaccuracies in the finite difference procedure. The T-mode is seen to be much more affected by the choice of (u, v)-interpolation quality, with frequencies varying from 54 to 108 cm^{-1} depending also on the proper treatment of dispersion corrections. We will see later that this sensitivity is caused by the extreme flatness of the PES in the plane parallel to the surface.

The importance of inter-mode coupling and anharmonicity can be assessed by computing the full-dimensional vibrational eigenstates of the system using a variational expansion of the wave functions. Here it turns out convenient to transform the Cartesian coordinates X and Y to the skewed u, v coordinates which reflect the symmetry of the hexagonal lattice (cf. Fig. 1). For the hexagonal lattice, $u = X - v/2$ and $v = Y2/\sqrt{3}$. The total Hamiltonian of the system reads then

$$\begin{aligned}\hat{H}_{vib}(u, v, Z, r, \theta, \phi) &= -\frac{\hbar^2}{2M}\frac{\partial^2}{\partial Z^2} \\ &-\frac{\hbar^2}{2M\sin^2(\alpha)}\left(\frac{\partial^2}{\partial u^2} - 2\cos(\alpha)\frac{\partial^2}{\partial u \partial v} + \frac{\partial^2}{\partial v^2}\right) \\ &-\frac{\hbar^2}{2\mu}\frac{\partial^2}{\partial r^2} - \frac{\hbar^2}{2\mu r^2}\hat{J}^2(\theta, \phi) + V(u, v, Z, r, \theta, \phi), \quad (6)\end{aligned}$$

where $\alpha = 60^\circ$ is the angle between u and v axes. Further, $M = m_C + m_O$ and $\mu = m_C m_O/M$ are the total mass and reduced mass of the system, respectively, and the other variables are as above. The Hamiltonian (6) was diagonalized using similar techniques as described elsewhere.[9] Specifically, using a hybrid basis of four-dimensional (4D) contracted functions for $\{Z, r, \theta, \phi\}$ and discrete variable representations (DVR) for u and v. The fully coupled wave functions are expanded as

$$\Psi_n(u, v, Z, r, \theta, \phi) = \sum_{i_u, i_v, i_{4D}} C^{(n)}_{i_u, i_v, i_{4D}} \varphi_{i_u}(u_{i_u})\, \varphi_{i_v}(v_{i_v})\, \varphi_{i_{4D}}(Z, r, \theta, \phi). \quad (7)$$

Plane wave DVR functions (exp-DVR) are used to evaluate the integrals along u and v while enforcing the proper translational symmetry. The four-dimensional basis functions $\varphi_{i_{4D}}(Z, r, \theta, \phi)$ are eigenfunctions of the Hamiltonian (6), fixed at the equilibrium point in the (u, v)-plane, expressed in a non-direct product basis of the form

$$\varphi_{i_{4D}}(Z, r, \theta, \phi) = \sum_{i_z, i_r, l, m} d^{(i_{4D})}_{i_z, i_r, l, m}\, \chi_{i_z}(Z_{i_z})\, \chi_{i_r}(r_{i_r})\, \Theta^m_l(\theta, \phi). \quad (8)$$

Here, the functions $\Theta^m_l(\theta, \phi)$ are normalized real spherical harmonics with Condon-Shortley phase factor, and $\{\chi_{i_z}(Z_{i_z}), \chi_{i_r}(r_{i_r})\}$ are potential-optimized DVR functions (PO-DVR) obtained from one-dimensional reference potentials for the Z and r coordinates, respectively.

Both the full-dimensional eigenfunctions and the contracted 4D bases are computed using a house implementation of the coupled two-term Lanczos algorithm with classical Gram-Schmidt re-orthogonalization.[9,57,58] To accelerate the vibrational analysis, we exploit the fact that the low-lying modes are almost adiabatically decoupled from the high-lying CO-stretch mode. First, we generate a 4D contracted basis using spherical harmonics up to $j_{\max} = 41$ and $m_{\max} = 6$, $N_z = 25$ PO-DVR bases along Z, and a single PO-DVR function along r. The 4D eigenfunctions obtained from 2000 Lanczos iterations are then combined with an equidistant grid representation of 35 × 35 points in the (u, v)-plane. Alternatively,

for extracting the high-lying CO-stretch mode frequency, the (u, v) coordinates are kept fixed at their equilibrium position and the basis along r is increased to 10 PO-DVR functions. The effect of changing the number of in-plane basis functions has been shown to be marginal for reduced dimensionality calculations on a similar system.[9] We choose to follow a similar approach here for computational efficiency.

The results are shown in the bottom part of Table II for the three different interpolation schemes ("QM"). All vibrational states have been assigned by visual inspection of the nodal structure of the eigenfunctions. At first, we note that the vibrational calculation recovers the proper two-fold degeneracy of R- and T-modes. Also, in all cases, the anharmonic vibrational frequencies are lower than determined by the NMA. Whereas the effect is only marginal for the T-mode, R-mode, and S-mode (<10 cm^{-1}), it is slightly more pronounced for the CO-stretch. Note that the latter does not change with varying (u, v) interpolation quality, which is an artifact of the present calculation as the u and v position are kept fixed. Since the CRP is a variational procedure, improving the quality of the (u, v) interpolation by adding more fitting functions should yield better results, which is obvious for the significant drop in the T-mode when going from the "low" to "medium" quality interpolation. This trend is paralleled by the NMA. Further, van der Waals corrections seem to improve the agreement with experimental results for the R- and S-modes, which are also shown in the table, whereas the T-mode is better represented with the pure RPBE PES. The experimental frequency for the S-mode seems rather insensitive on coverage,[55] while the CO-stretch (r-) mode is very sensitive to coverage—the value shown in the table is for a coverage of 0.25.[56] Although the results are quite satisfactory, the remaining discrepancies can be attributed to either the choice of density functional, which has been shown to underbind adsorbates in some cases, or the inclusion of only two-body terms in the D2 dispersion correction. Further, the rigid surface approximation will have an effect, too. A systematic analysis of the higher excited states, as well as the resonances located above the diffusion barrier, is beyond the scope of this work and will be the subject of a latter investigation.

VI. FEATURES OF THE POTENTIAL ENERGY SURFACE

We finally discuss a few features of the PES in more detail. In Fig 4, four different two-dimensional (2D) potential cuts along r and Z are plotted for different orientations of the molecular axis along θ. The center of mass position is fixed *on-top* of a Ru atom and $\phi = 0$.

In panel (a), the global minimum is marked which corresponds to a molecule aligned perpendicular to the surface with the C atom closer to the surface than the O atom, and with the geometrical parameters already specified in Sec. II. Here it suffices to say that the slight CO bond elongation from 1.15 Å in the gas phase to 1.17 Å in the adsorbed state, is due to the usual synergetic bonding mechanism, in particular the back donation of metal d-electrons into the unoccupied $2\pi^*$-orbital of CO. With increasing r the potential becomes quickly repulsive which is due to shortening of the C-Ru distance for this particular orientation.

In panels (b)–(d), we plot 2D cuts along r and Z when the molecule is rotated along the cartwheel mode θ while the center of mass position is still fixed *atop*. With increasing θ, the potential in the adsorption/desorption channel becomes more and more repulsive accompanied by the opening of the dissociation channel for CO indicated by the emergence of the "elbow" character of the potential. The dissociation energy of CO at the surface is remarkably reduced by about 6.5 eV, from 11.24 eV in the gas phase to 4.87 eV. This is the height

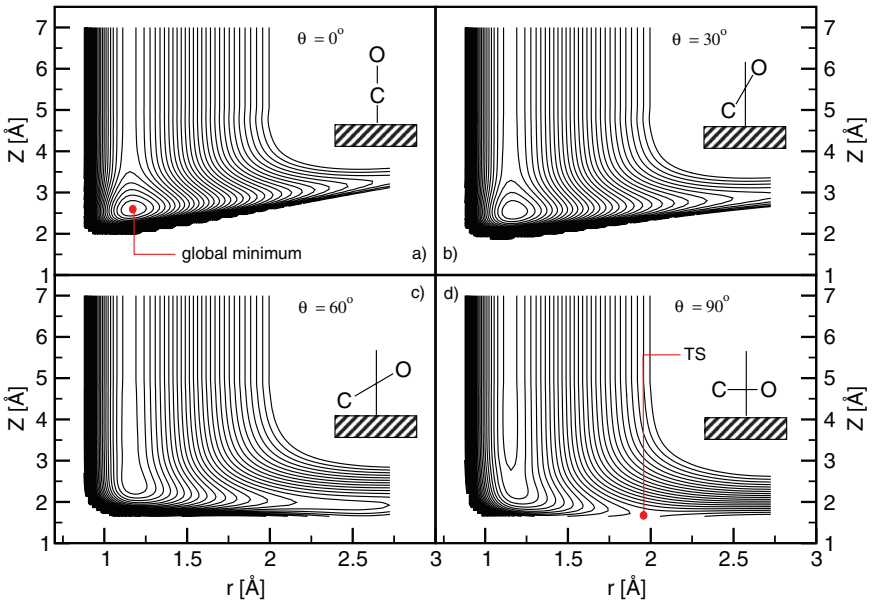

FIG. 4. Potential energy cuts for Ru(0001)(2×2):CO along r- and Z-coordinates calculated with V_{high} and vdW corrections. Shown are cuts for (a) $\theta = 0°$, (b) $\theta = 30°$, (c) $\theta = 60°$, and (d) $\theta = 90°$. The center of mass is located at *top* position and $\phi = 0°$. In panel (a) the global minimum is marked and in panel (d) the transition state for a dissociating CO molecule. Contour plots are made for $V \in [0, 10]$ eV and a line separation of 300 meV.

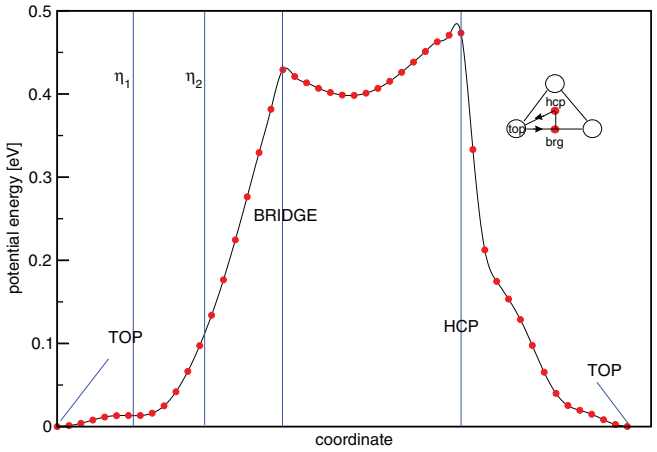

FIG. 5. Potential energy for CO moving from *top* → *bridge* → *hcp* → *top* (see also inset). All coordinates not related to this motion were free to relax.

of the transition state (TS) towards dissociation, relative to the global minimum. The TS is indicated in panel (d), at $Z = 1.65$ Å and $r = 1.89$ Å. We note that the surface is highly corrugated and that many different transition states for CO dissociation exist which vary in location and height. For example, letting the C atom fixed *atop* and moving the O atom along X, the TS is found at larger Z and r distances, namely, $Z = 1.75$ Å and $r = 2.05$ Å, with the barrier of 4.70 eV. Considering an O atom fixed *atop* and the C atom moving along X, we obtain a TS at a similar surface molecule distance but at $r = 2.22$ Å, exhibiting an even lower activation energy of about 4.52 eV. For the latter cases, DFT calculations yield very similar energies at these geometries, that is, 4.74 eV and 4.51 eV, which deviate by +43 meV and −10 meV, respectively, from the CRP values.

In Sec. V, a flat potential at the global minimum geometry was indicated by low vibrational frequencies for the X and Y motion. In Fig. 5, we visualize this in more detail. Shown is the potential energy for CO moving straight from *top* to the *bridge* site, then from *bridge* to *hcp* and from *hcp* back to *top*. All degrees of freedom being not related to this motion were relaxed adiabatically.

As one can see, for small distances between the center of mass position and the *top* site, the potential increases only slightly: At η_1 ($X \approx 0.454$ Å), the potential energy is about 12 meV, and at η_2 ($X \approx 0.91$ Å) about 112 meV. The flatness of the potential can be well explained by looking at the angular orientation of the molecular axis during the lateral motion: While r and Z do not vary dramatically, the molecule changes its molecular orientation from the perpendicular to a tilted form. The cartwheel coordinate θ rises quickly from 0° to 23°. This behaviour increases the stability of the C-Ru bond at any given position on the surface by maximizing the back bonding between the metal d-electrons and the unoccupied $2\pi^*$-orbital of the CO molecule. As the molecule moves along the surface, this increased overlap compensates for the weaker direct C-Ru bond and, consequently, the potential remains almost unchanged. At the *bridge* site, a diffusion barrier of 430 meV is found which increases up to 470 meV at the *hcp* site. Experimentally, a value of 480 meV was determined.[59] This shows that the dynamics of the CO molecule is mostly confined in the vicinity of the *atop* position, where it moves almost freely. Within the rigid surface approximation, this will hold even true at moderate adsorbate temperatures.

VII. CONCLUSIONS

In this work, we have presented a new six-dimensional potential energy surfaces for CO adsorbed on a Ru(0001) surface, at a coverage of 1/4. The energies of about 90 000 geometries for the CO molecule calculated with periodic DFT, the RPBE functional and, additionally, with vdW corrections were considered. Three different interpolation schemes were developed with different numbers of adsorption sites that were included in the interpolation, giving three flavours of the potential, V_{low}, V_{med}, and V_{high} with increasing accuracy. The corrugation reducing procedure (CRP) performs excellent also for this heteronuclear molecule, certainly at energies $\lesssim$3 eV, and the resulting PES curves are in very good agreement with DFT reference energies. This is even true for the less accurate potentials V_{low} and V_{med} which show only small deviations from V_{high}. For dynamical purposes, a dense grid of the potential along the (u, v)-plane seems not to be essential. However, when sensitive quantities such as vibrational frequencies are of interest a highly accurate potential is needed. This might be a special feature for systems where the global minimum geometry is associated with a flat potential.

Currently, the evaluation of details of vibrational features of Ru(0001)(2×2):CO and hot-electron driven molecular dynamics in this system, using the new CRP PES potential, are underway in our laboratory.

ACKNOWLEDGMENTS

This work was funded by the Deutsche Forschungsgemeinschaft through project Sa 547/8-1, and in part by the Leibniz Graduate School "Dynamics in new Light (DinL)."

[1] A. H. Zewail, Science **242**, 1645 (1988).
[2] T. Klüner, Prog. Surf. Sci. **85**, 279 (2010).
[3] J. Greeley, J. K. Nørskov, and M. Mavrikakis, Annu. Rev. Phys. Chem. **53**, 319 (2002).
[4] G.-J. Kroes, Prog. Surf. Sci. **60**, 1 (1999).
[5] A. Groß, Surf. Sci. Rep. **32**, 291 (1998).
[6] G. Füchsel, T. Klamroth, S. Monturet, and P. Saalfrank, Phys. Chem. Chem. Phys. **13**, 8659 (2011).
[7] G. Füchsel, J. C. Tremblay, T. Klamroth, P. Saalfrank, and C. Frischkorn, Phys. Rev. Lett. **109**, 098303 (2012).
[8] C. Diaz, E. Pijper, R. A. Olsen, H. F. Busnengo, D. J. Auerbach, and G. J. Kroes, Science **326**, 832 (2009).
[9] R. Marquardt, F. Cuvelier, R. A. Olsen, E. J. Baerends, J. C. Tremblay, and P. Saalfrank, J. Chem. Phys. **132**, 074108 (2010).
[10] G. C. Schatz, Rev. Mod. Phys. **61**, 669 (1989).
[11] G. Wiesenekker, G. J. Kroes, and E. J. Barends, J. Chem. Phys. **104**, 7344 (1996).
[12] C. Crespos, M. A. Collins, E. Pijper, and G. J. Kroes, Chem. Phys. Lett. **376**, 566 (2003).
[13] M. Luppi, R. A. Olsen, and E. J. Baerends, Phys. Chem. Chem. Phys. **8**, 688 (2006).
[14] C. Diaz, R. A. Olsen, H. F. Busnengo, and G. J. Kroes, J. Phys. Chem. C **114**, 11192 (2010).
[15] H. F. Busnengo, A. Salin, and W. Dong, J. Chem. Phys. **112**, 7641 (2000).
[16] J. Behler, Phys. Chem. Chem. Phys. **13**, 17930 (2011).
[17] B. G. Sumpter and D. W. Noid, Chem. Phys. Lett. **192**, 455 (1992).

[18]S. Lorenz, A. Groß, and M. Scheffler, Chem. Phys. Lett. **395**, 210 (2004).
[19]S. Manzhos and K. Yamashita, Surf. Sci. **604**, 555 (2010).
[20]S. Manzhos and T. Carrington, Jr., J. Chem. Phys. **125**, 084109 (2006).
[21]S. Manzhos and T. Carrington, Jr., J. Chem. Phys. **127**, 014103 (2007).
[22]D. E. Starr and H. Bluhm, Surf. Sci. **608**, 241 (2013).
[23]J. Gladh, T. Hansson, and H. Öström, Surf. Sci. **615**, 65 (2013).
[24]L. Diekhner, H. Mortensen, A. Baurichter, and A. C. Luntz, J. Chem. Phys. **115**, 3356 (2001).
[25]S. Wagner, H. Öström, A. Kaebe, M. Krenz, M. Wolf, A. C. Luntz, and C. Frischkorn, New J. Phys. **10**, 125031 (2008).
[26]C. Corriol, G. R. Darling, S. Holloway, I. Brenig, W. Andrianov, T. Klamroth, and P. Saalfrank, J. Chem. Phys. **117**, 4489 (2002).
[27]C. Corriol, G. R. Darling, S. Holloway, I. Andrianov, T. Klamroth, and P. Saalfrank, Surf. Sci. **528**, 27 (2003).
[28]J.-S. McEwen and A. Eichler, J. Chem. Phys. **126**, 094701 (2007).
[29]H. Pfnür, P. Feulner, and D. Menzel, J. Chem. Phys. **79**, 4613 (1983).
[30]S. Wurm, P. Feulner, and D. Menzel, Phys. Rev. Lett. **74**, 2591 (1995).
[31]M. Bonn, S. Funk, C. Hess, D. N. Denzler, C. Stampfl, M. Scheffler, M. Wolf, and G. Ertl, Science **285**, 1042 (1999).
[32]K. L. Kostov, H. Rauscher, and D. Menzel, Surf. Sci. **278**, 62 (1992).
[33]C. Stampfl and M. Scheffler, Phys. Rev. B **65**, 155417 (2002).
[34]M. Dell'Angela, T. Anniyev, M. Beye, R. Coffee, A. Föhlisch, J. Gladh, T. Katayama, S. Kaya, O. Rupin, A. Møgelhøj, D. Nordlund, J. K. Nørskov, H. Öberg, H. Ogasawara, H. Öström, L. G. M. Petterson, W. F. Schlotter, J. A. Sellberg, F. Sorgenfrei, J. Turner, M. Wolf, W. Wurth, and A. Nilsson, Science **339**, 1302 (2013).
[35]G. Füchsel, T. Klamroth, J. C. Tremblay, and P. Saalfrank, Phys. Chem. Chem. Phys. **12**, 14082 (2010).
[36]G. Volpilhac, H. F. Busnengo, W. Dong, and A. Salin, Surf. Sci. **544**, 329 (2003).
[37]D. A. McCormack, R. A. Olsen, and E. J. Baerends, J. Chem. Phys. **122**, 194708 (2005).
[38]M. Alducin, R. Díez Muiño, H. F. Busnengo, and A. Salin, J. Chem. Phys. **125**, 144705 (2006).
[39]G. Kresse and J. Furthmüller, Phys. Rev. B **54**, 11169 (1996).
[40]G. Kresse and D. Joubert, Phys. Rev. B **59**, 1758 (1999).
[41]J. P. Perdew, K. Burke, and M. Ernzerhof, Phys. Rev. Lett. **77**, 3865 (1996).
[42]P. E. Blöchl, Phys. Rev. B **50**, 17953 (1994).
[43]R. L. Clendenen and H. G. Drickamer, J. Phys. Chem. Solids **25**, 865 (1964).
[44]M. Wijzenbroek and G. J. Kroes, J. Chem. Phys. **140**, 084702 (2014).
[45]S. Grimme, J. Comput. Chem. **27**, 1787 (2006).
[46]E. McNellis, J. Meyer, and K. Reuter, Phys. Rev. B **80**, 205414 (2009).
[47]H. Over, W. Moritz, and G. Ertl, Phys. Rev. Lett. **70**, 315 (1993).
[48]B. deB. Darwent, Natl. Stand. Ref. Data Ser. **31**, 23 (1970).
[49]N. Sathyamurthy and L. M. Raff, J. Chem. Phys. **63**, 464 (1975).
[50]R. A. Olsen, H. F. Busnengo, A. Salin, M. F. Somers, G. J. Kroes, and E. J. Baerends, J. Chem. Phys. **116**, 3841 (2002).
[51]E. D. William, E. H. Weinberg, and A. Sobrero, J. Chem. Phys. **76**, 1150 (1982).
[52]M. Gierer, H. Bludau, H. Over, and G. Ertl, Surf. Sci. **346**, 64 (1996).
[53]P. Jakob, J. Chem. Phys. **108**, 5035 (1998).
[54]C. Hess, S. Funk, M. Bonn, D. Denzler, M. Wolf, and G. Ertl, Appl. Phys. A **71**, 477 (2000).
[55]G. Thomas and W. Weinberg, J. Chem. Phys. **70**, 1437 (1979).
[56]H. Pfnür, D. Menzel, F. Hoffmann, A. Ortega, and A. Bradshaw, Surf. Sci. **93**, 431 (1980).
[57]J. C. Tremblay and T. Carrington, Jr., J. Chem. Phys. **125**, 094311 (2006).
[58]J. C. Tremblay, S. Beyvers, and P. Saalfrank, J. Chem. Phys. **128**, 194709 (2008).
[59]A. Deckert, J. L. Brand, M. V. Arena, and S. M. George, Surf. Sci. **208**, 441 (1989).